

AN ELECTRON SYNCHROTRON LATTICE BASED ON THEORETIC MINIMAL EMITTANCE CELL

H.-C. Chao*, DESY, Hamburg, Germany

Abstract

A design of an electron synchrotron featuring the theoretic minimal emittance (TME) cells is presented. It has 32 superperiods and the circumference is around 300 m. It offers versatile functions with the equilibrium emittance less than 10 nm-rad at 6 GeV. The beam energy can go up to 7.5 GeV. Locations with proper phase advances are found to form effective vertical orbit bumps, which can be used for the injections and extraction. A tune scan study shows the sweet spot for the working point. Some discussions of other usages and studies of synchro-betatron coupling (SBC) effects are also included in this article.

INTRODUCTION

The PETRA IV project toward a diffraction limit synchrotron light source at 6 GeV features an ultra low emittance storage ring. It has a very small dynamic aperture (DA) so the beam to be injected must have very low emittance. The current booster DESY II having FODO lattice does a good job preparing the beam to be injected and accumulated in PETRA III. It has been in service for more than 50 years and is still reliable. However, its emittance (350 nm-rad) is too large for PETRA IV so a new synchrotron is always needed as a booster or an accumulator. It has to be in the existing old tunnel which can accommodate rings of sizes between 292 to 316 m. The key goal of the injector upgrade project is to achieve the equilibrium emittance < 30 nm-rad at 6 GeV [1].

A natural approach to small emittance lattice is to use more bending magnets. Besides, combining gradient field components into bending magnets can not only save more space for magnets, but also repartition the damping partition to reach further small horizontal natural emittance. For example, a well designed booster synchrotron in the previous study [2] offers the equilibrium emittance as low as 19 nm-rad at 6 GeV and enough number of straights with enough lengths for different purposes. It features the FODO lattice with the combined function bending magnets.

This study addresses another type of lattice which features TME cells and vertical orbit bumps for injection and extraction. This article is organized as follows. Firstly the TME lattice is defined and a systematic study of tune scan is carried out. Then a good working point is chosen for large vertical DA. Locations for an efficient vertical orbit bump for injection and extraction are also found. The ring parameters are listed and some beam dynamics behaviors simulated. The versatile functions are discussed. Finally, the SBC effect are simulated and some conclusions are given.

* hung-chun.chao@desy.de

TME CELL

The optimum Twiss parameter values for minimizing the natural emittance ε in the case of a pure bending magnet of length L and deflection angle θ are $\beta^* = \frac{L}{2\sqrt{15}}$ and $D^* = \frac{L\theta}{24}$ in the symmetric point of the magnet [3, 4]. Under these conditions, the minimal is $\varepsilon_{x0}^* [nm - rad] = 1470 \frac{(E[GeV])^2}{J_x} \frac{\theta^3}{12\sqrt{15}}$. Assuming N_p pure dipole bending magnets are used in the ring, the relation $J_x \approx 1$ holds. Plugging in the energy $E = 6$ GeV and $\theta = 2\pi/N_p$, we have $\varepsilon_{x0}^*(N_p = 36) = 6.1$ nm-rad, $\varepsilon_{x0}^*(N_p = 32) = 8.6$ nm-rad, and $\varepsilon_{x0}^*(N_p = 30) = 10.5$ nm-rad.

Considering the constraints from the existing tunnel and the small emittances requirement, we will stick on the geometry of a 292.8-m circumference ring with the superperiodicity $N_p = 32$ in this study. The lattice and linear optics of this TME cell are depicted in Fig. 1.

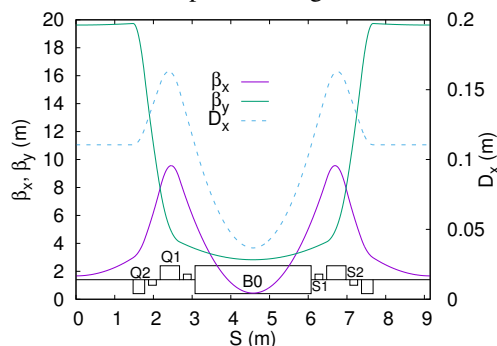


Figure 1: Twiss functions in one superperiod.

The magnet section consists of one dipole, 4 quadrupoles and 4 sextupoles. The dipoles are 3-meter long and run at 1.31 Tesla at 6 GeV. Two pairs of quadrupoles of lengths 50 cm and 30 cm next to the dipole are used to control the Twiss parameters. Two families of sextupoles of lengths 20 cm are inserted in the locations with large beta function differences for the efficient chromaticity correction. The gaps between magnets are 10 cm. Roughly speaking, bending magnets occupy one third of the circumference and straight sections another one third.

TME32 RING

The ring is constructed by 32 of such cells. Therefore it is named TME32. There are in total 32 dipoles, 128 quadrupoles, and 128 sextupoles (or less). Its linear lattice parameters are listed in Table 1.

This lattice provides as many as 32 2.95-meter straights for various purposes. They can accommodate many RF modules, injection/extraction elements, and other elements such as harmonic cavities, skew quadrupoles, Robinson wigglers, etc for the beam manipulations.

Table 1: TME32 Parameters

| Property | TME32 |
|--|----------------------|
| Circumference | 292.8 m |
| Harmonic Number | 488 |
| Ramping Repetition Rate | 2-5 Hz |
| Working Tune (H/V) | 23.20/8.30 |
| Natural Chromaticity (H/V) | -39.4/-34.6 |
| Momentum Compaction | $1.3 \cdot 10^{-3}$ |
| at Beam Extraction Energy 6 GeV | |
| Energy Loss Per Turn | 7.5 MeV |
| Equilibrium Emittance | 9.9 nm-rad |
| Equilibrium Energy Spread | $1.31 \cdot 10^{-3}$ |
| Damping Time (H/V/L) | 1.6/1.6/0.8 ms |

TME32 can offer versatile functions. It can be not only a booster for PETRA IV, but also an accumulator. Moreover, it can be a recycler to accept and accumulate the bunches swapped out from PETRA IV. The beam can be then re-used or decelerated to dump at lower energy. Furthermore, it can be operated at other energies for different purposes. This will offer the platform for the future R&D and the applications of laser plasma wake field accelerators and some Test beamlines for the detector development [5].

Quadrupole and Sextupole Strengths

This lattice configuration has a very good tunability on linear optics. A systematic scan of linear optics solutions of this lattice configuration is carried out. By keeping the chromaticities $(\xi_x, \xi_y) = (+1, +1)$ with two families of sextupoles, their strengths are uniquely determined. The contours of quadrupole and sextupole strengths are shown in Fig. 2. Their strengths are moderate at 6 GeV and saturate at 7.5 GeV.

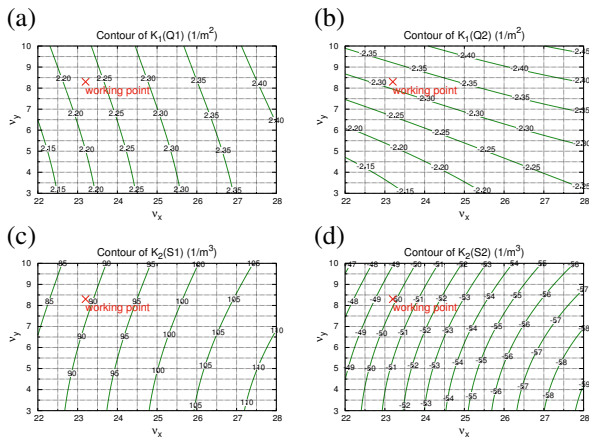


Figure 2: Contour of quadrupole and sextupole strengths: (a) Q1, (b) Q2, (c) S1, (d) S2. ($K_2 \equiv \frac{1}{B\rho} \frac{\partial^2 B_y}{\partial x^2}$).

Emittance and Twiss Functions

The contours of the natural emittance ϵ_{x0} at 6 GeV and the Twiss parameters β_x, β_y, D_x in the straight centers in

the tune space are also shown in Fig. 3. From these plots we can observe some general behaviors.

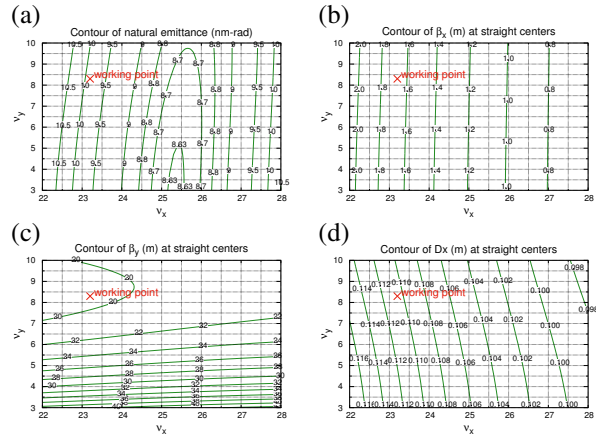


Figure 3: Contours of (a) ϵ_{x0} , (b) β_x , (c) β_y , and (d) D_x .

Figure 4 shows the iso-emittance contours in (b, d) parameterization [6] which are defined by the beta function and dispersion normalized with β^* and D^* . The emittance is near the theoretic minimal emittance ($F = 1$).

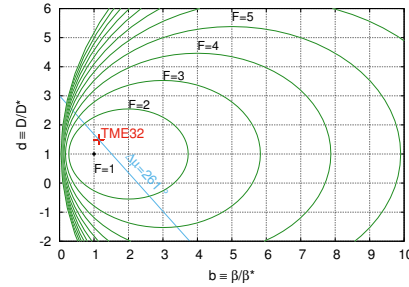


Figure 4: The elliptic iso-emittance contours.

Tune Spreads Coefficients

The large range tune diagram with systematic resonances of $N_p = 32$ is shown in Fig. 5(a). Figure 5(b)-(d) show the scaled absolute values of detuning factors, where the first order tune detuning factors $\alpha_{xx}, \alpha_{xy}, \alpha_{yy}$ w.r.t. the particle actions J_x and J_y are defined as

$$\begin{aligned} \Delta \nu_x &= \alpha_{xx} J_x + \alpha_{xy} J_y, \\ \Delta \nu_y &= \alpha_{xy} J_x + \alpha_{yy} J_y. \end{aligned}$$

Smaller detuning factors means the more localized tune spread of particles with different actions, therefore larger DA. The colder color stands for the lower values. The valleys of low detuning values can be observed. To have large vertical DA, at least α_{xy} and α_{yy} have to be small. In this design α_{xx} is less important than others. Their intersection in the half integer tune window $23 < \nu_x < 23.5$ and $8.0 < \nu_y < 8.5$ is the sweet spot for larger vertical dynamic apertures. There is no systematic resonance within this tune window.

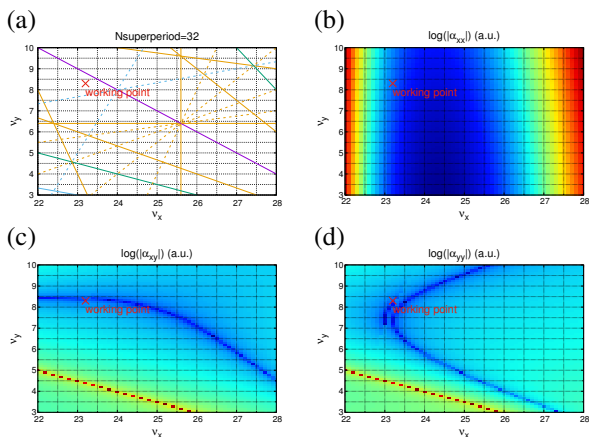


Figure 5: (a) Tune diagram and scaled detuning factors: (b) α_{xx} , (c) α_{xy} , (d) α_{yy} .

Dynamic Aperture

The chosen working point $(\nu_x, \nu_y) = (23.2, 8.3)$, indicated as the red cross, is not too far away from the condition of optimal vertical dynamic apertures. It is slightly away from the TME condition though. At this point, the detuning factors, calculated by Lie algebra method with LEGO [7], are $(\alpha_{xx}, \alpha_{xy}, \alpha_{yy}) = (-35976, -297, -441)$ [1/m]. The chromatic tune shift for $\delta = 5\%$ is less than 0.25 horizontally and less than 0.05 vertically.

The DA and the frequency map with tune diffusion rate tracked by Elegant [8] are shown in Fig. 6. As a consequence, the vertical DA is large enough for vertical injection. The horizontal DA is limited by the integer resonance and is within $|DA_x| < 3$ mm.

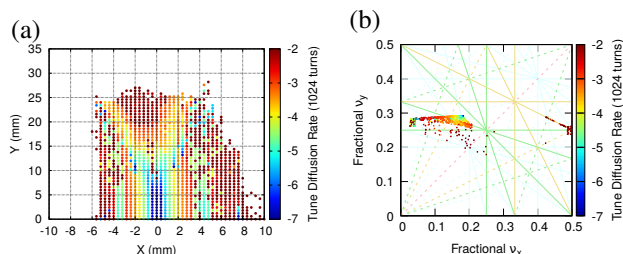


Figure 6: (a) Dynamic aperture and (b) Frequency map.

INJECTION AND EXTRACTION

This lattice configuration features low β_x in the straights. Therefore the horizontal DA is limited and the horizontal orbit deviation by kickers or bumpers is inefficient. Fortunately, β_y is relatively large in the straights so it can be utilized to design the injection and extraction.

Vertical Orbit Bump

A simple local orbit bump can be formed by two bumpers at the locations with identical beta functions and a phase advance difference $\Delta\phi = \pi$. Two ideal locations for a vertical orbit bump are found as plotted in Fig. 7. The first is at the end of a straight, while the second is at the front of the straight two sections downstream. In between two magnet

sections and one full straight are sandwiched. A Lambertson septum can be installed in the straight. The leverage of the bump is very efficient with $r = 19.6$ mm/mrad. This enables its ability accumulate the beams at higher energy. Throughout the whole ring there are at most 16 slots for this kind of local bump. These bumps can be utilized for the injection and extraction.

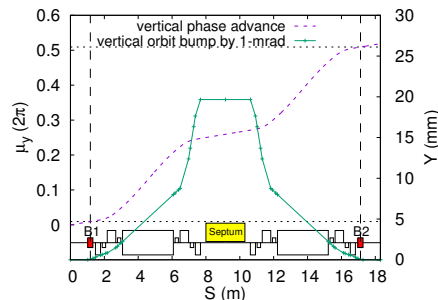


Figure 7: Every two cells have a vertical π -bump.

The bump orbit may be altered by the sextupoles through which the trajectory goes but it can always be fixed easily by correctors, which can be built in sextupoles. Some magnets have to be properly designed so that injection/extraction trajectory can go through them without being blocked.

SYNCHRO-BETATRON COUPLING

The SBC effect also affects the beam emittance. Its driving mechanism is from the forces depending on momentum or on the longitudinal position in the bunch. In this case, the major contribution comes from the dispersion in RF sections since the cavities are located in non-achromat sections. Implemented by the analytic formulas [9], the equilibrium emittance growth rates at different tunes are shown in Fig. 8. Conclusively, the emittance growth is negligible due to its small synchrotron tune. SBC caused by dispersive RF cavities is harmless.

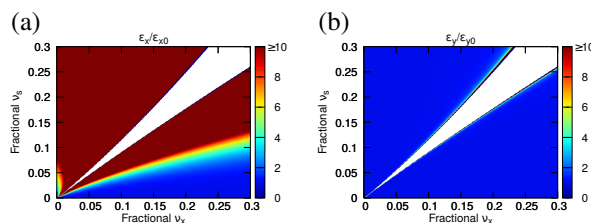


Figure 8: Relative emittance growths: (a) horizontal, (b) vertical. The white region stands for the instability.

CONCLUSION

The goal of designing a low emittance synchrotron with TME lattice is achieved. With 32 superperiods, its equilibrium emittance is about 10 nm-rad at 6 GeV, just 15% more than the TME condition. It can be an option of the booster or accumulator for the PETRA IV project. Moreover, its energy can go up to 7.5 GeV and many other versatile usages are possible.

REFERENCES

- [1] C. G. Schroer *et al.*, “PETRA IV: upgrade of PETRA III to the Ultimate 3D X-ray microscope. Conceptual Design Report”, Deutsches Elektronen-Synchrotron DESY, Hamburg, Germany, Rep. PUBDB-2019-03613, 2019.
- [2] H.-C. Chao, “Design Status of DESY IV – Booster Upgrade for PETRA IV”, in *Proc. IPAC’19*, Melbourne, Australia, May 2019, pp. 331–334. doi:10.18429/JACoW-IPAC2019-MOPGW092
- [3] L. C. Teng, “Minimum emittance Lattice for Synchrotron Radiation Storage Rings”, IL, USA, *Tech. Rep. ANL-LS-17*, 1985.
- [4] J. P. Delahaye and J. P. Potier, “Study of Lattices Optimised for Small Emittances and Storage Damping”, CERN, Geneva, Switzerland, *CERN/PS/91-10*, CLIC Note 130, 1991.
- [5] R. Diener *et al.*, “The DESY II test beam facility”, *NIM-A*, vol 922, p. 265, April 2019. doi:10.1016/j.nima.2018.11.133
- [6] S. C. Leemann and A. Streun, “Perspectives for future light source lattices incorporating yet uncommon magnets”, *Phys. Rev. ST Accel. Beams*, vol. 14, no. 3, Mar. 2011. doi:10.1103/physrevstab.14.030701
- [7] Y. Cai, “LEGO: A Class library for accelerator design and simulation”, *SLAC-PUB-8011*, Menlo Park, CA, 1998.
- [8] M. Borland, “elegant: A Flexible SDDS-Compliant Code for Accelerator Simulation”, Argonne National Lab., IL, USA, Rep. LS-287, Sep. 2000.
- [9] B. Nash, J. Wu, and A. W. Chao, “Equilibrium beam distribution in an electron storage ring near linear synchrotron coupling resonances”, *Phys. Rev. ST Accel. Beams*, vol. 9, no. 3, p. 032801, Mar. 2006.